From bio-waste to biomaterials: insect eggshells as templates for SERS-active surfaces

Lian-Sheng Zang[a], Yong-Ming Chen[a], Behlul Koc-Bilican[b,c], Ismail Bilican[c,d,e], Menekse Sakir[f], James Wait[g], Arzu Colak[g], Tugce Karaduman[b], Ahmet Ceylan[h], Asad Ali[i], Caglar Elbuken[e,j], M. Serdar Onses[e,f,k,*], Murat Kaya[b,d,*]

[a] *Key Laboratory of Green Pesticide and Agricultural Bioengineering, Guizhou University, 550025 Guiyang, China*
[b] *Department of Biotechnology, Faculty of Science and Letters, Aksaray University, 68100 Aksaray, Turkey*
[c] *ASUBTAM-Science and Technology Application and Research Center, Aksaray University, 68100 Aksaray, Turkey*
[d] *Department of Electronics and Automation, Technical Vocational School, Aksaray University, 68100 Aksaray, Turkey*
[e] *UNAM—National Nanotechnology Research Center, Institute of Materials Science and Nanotechnology, Bilkent University, 06800 Ankara, Turkey*
[f] *ERNAM - Erciyes University Nanotechnology Application and Research Center, 38039 Kayseri, Turkey*
[g] *Department of Physics, Faculty of Arts and Sciences, Clarkson University, 13699 New York, USA*
[h] *Department of Pharmaceutical Biotechnology, Faculty of Pharmacy, Erciyes University, 38280, Kayseri, Turkey*
[i] *Department of Agriculture, Abdul Wali Khan University, Mardan, 23200 Khyber Pakhtunkhwa, Pakistan*
[j] *Faculty of Biochemistry and Molecular Medicine, Faculty of Medicine, University of Oulu, 90014 Oulu, Finland*
[k] *Department of Materials Science and Engineering, Erciyes University, Kayseri, 38039 Turkey*

Corresponding Author

M. Serdar Onses
* Address: ERNAM - Erciyes University Nanotechnology Application and Research Center, 38039, Kayseri, Turkey
E-Mail: onses@erciyes.edu.tr
Tel.: +90 352 207 6666 (13802)

Murat Kaya
* Address: Aksaray University, Faculty of Science and Letters, Department of Biotechnology, 68100, Aksaray, Turkey.
E-Mail: muratkaya3806@yahoo.com
Tel.: +90-382-288-2216

Abstract

Although over 80% of the world's existing animal species are insects, with each of these species having unique eggshell morphologies, limited information is available regarding the use of their eggshells in material science applications. The present research discusses using discarded eggshells of the Chinese oak silkworm (*Antheraea pernyi*) as a technological material. These insects are reared on a large scale in natural enemy production facilities as a factitious host for *Trichogramma* parasitoids for use in biological control programs involving a number of insect pests. The 3-dimensional aspects of the insect's eggshell were examined in detail, demonstrating the complexity of their novel surface morphology. The outer surface of the eggshell was comprised of a hexagonal structure, whereas the inner surface consists of a mostly smooth surface. Distinctive layers of the eggshell were observed when cross sections of the surface were analyzed. The elastic modulus of the inner part of the eggshell is substantially greater than that of the outer part. The physicochemical properties of the eggshell were characterized and no toxic properties were found. The hexagonal structures found on the outer surface of the eggshell provide a highly suitable template for silver nanostructure deposition. The resulting silver decorated surfaces can be used to detect molecules via surface-enhanced Raman scattering (SERS) effects. The deposition of silver renders the surface antimicrobial, whereas the original surface was microbial. As a result, it will be possible to utilize the insect eggshells in industrial SERS applications.

Keywords: Bio-waste; oak silkworm; *Antheraea pernyi*; 3D assembly; materials science; non-toxic; SERS

Introduction

Insects are recognized as the most biodiverse group in the animal kingdom with more than 80% of the world's existing animal species in the world belonging to the class Insecta [1]. Every insect taxon has its own unique eggshell morphology. Insect eggshells generally consist of a substance referred to as chorion protein [2,3]. These shells have an ideal design that prevents water penetration while permitting the oxygen exchange and carbon dioxide release required for embryonic development. The shell also minimizes the loss of water in the egg, preventing desiccation [4,5]. Previous studies on insect eggshells have focused primarily on specific morphological adaptations useful in species identification and phylogenetic studies, identification of eggshell layers, their structural protein content, and the genes that are involved in the production of the proteins [6-10]. Interestingly, insect eggshells, involving an abundance of species and diverse surface morphologies, have not previously been studied in terms of materials science.

The diverse morphology and protein-rich composition of insect eggshells provide a suitable template for the fabrication of functional surfaces. Technologically important materials are plasmonically active surfaces with broad application potentials ranging from sensing to anti-counterfeiting [11-13]. The strong confinement of light near metallic nanostructures is the basis of plasmonically active surfaces. The spatial organization of metallic nanostructures is critical, since the inter-particle distances play an important role in the generation of plasmonic hot-spots, where strong electromagnetic fields are present [14,15]. One attractive characteristic of these plasmonic hot-spots is the enhancement of inelastic scattering of light in Raman spectroscopy [16]. Commonly referred to as surface-enhanced Raman scattering (SERS) spectroscopy, this approach has strong potential in biosensing applications in forensic and food science, environment monitoring, drug analysis, security labelling, and biotechnology [17-23]. We

hypothesize that insect eggshells may serve as a suitable platform for SERS studies for two reasons. First, the functional groups present on the surface of insect eggshells exhibit reactive sites for in-situ growth of metallic nanostructures. Second, the morphology of insect eggshells can provide the necessary structural guidance for the generation of plasmonic-hot spots. The in-situ growth of metallic nanostructures is performed using different strategies for maximizing the SERS activity of insect eggshells. Picomolar level sensing of probe molecules was accomplished based on novel dye-assisted growth of silver nanostructures mediated by the substantial dye absorption characteristic of insect eggshells.

The Chinese oak silkworm (COS) *Antheraea pernyi* (Guérin-Méneville) (Lepidoptera: Saturniidae) has been domesticated for at least two thousand years in China [24]. COS eggs are used as a host in the mass production of parasitic wasps, including species in the genera *Trichogramma*, *Anastatus*, *Mesocomys*, *Aprostocetus*, *Ooencyrtus*., etc. [25,26]. *Trichogramma* parasitoids have been produced through mass rearing of COS eggs since the 1960s [27]. Currently, COS eggs are among the best factitious hosts for mass producing *Trichogramma* parasitoids in China [28]. COS eggs are large, averaging 3180 μm x 2684 μm in size, and are capable of producing between 50 to 260 *Trichogramma* wasps per egg [29]. China has developed and industrialized a mass-rearing technique for cost-effective production of *Trichogramma* parasitoids based on the use of COS eggs as an alternative host. A single production line is capable of producing 200 billion wasps per year for use in biological control of agricultural and forestry pests [30]. During the mass production of *Trichogramma*, regardless of whether they are produced by first generation female parasitoids or their offspring, tons of COS eggshells are discarded as waste every year. In order to consider using this insect bio-waste in the industry, it is our intension to introduce these eggshells for SERS sensing applications. To accomplish this, we first elucidated the gross morphology of the external and

internal structures of the eggshell. Then, cell adhesion, physicochemical characterization and toxicity test of the eggshells were performed. Finally, the hexagonal structures found on the outer surface of the eggshell were used as a substrate for adhesion of silver nanostructures.

Experimental sections

Materials

The waste eggs shells of *A. pernyi* were obtained from Jilin Agricultural University, Changchun, China. Female *A. pernyi* moths were collected after emerging from cocoons collected in Yongji (Jilin Province) China. The eggs used for parasitization by the wasps were dissected from the abdomens of unmated mature female moths, washed with distilled water and then air-dried at room temperature. After the *Trichogramma* parasitoids had emerged, the waste eggshells were collected and used for the experiments (Fig. S1).

The waste COS eggshells were washed several times with distilled water to remove possible contaminants. The eggshells were then treated with 0.5 M NaOH at 50 ° C for 10 min to remove the attached residual protein layer. To remove the used base, the eggshell material was washed with distilled water until reaching a neutral pH. Finally, the samples were dried in an oven at 60 °C for 24 hr.

Characterization

Infrared spectra of COS eggshells were obtained using a Perkin Elmer Spectrum Two FT-IR Spectrometer fitted with a Universal Attenuated Total Reflectance at 8 cm^{-1} resolution in the wavelength range of 600-4000 cm^{-1}. Ten scans were averaged to improve the signal-to-noise ratio.

Thermal stabilities of the COS eggshells were performed using TGA Exstar-TG/DTA 7300 Instruments. Analyses were conducted under a nitrogen atmosphere at a heating rate of 10 °C/min between 30-730 °C using a platinum crucible.

The surface morphologies of the COS eggshells were determined using SEM analysis at 5 kV at a range of 500X-30.000X. The samples were gold-plated before the analysis with a Cressington 108 Auto sputter coater, (Ted Pella, Inc.) Energy dispersion spectra (EDS) were obtained at 20 kV and 5000X magnification (EDAX Octane Pro).

Elemental analysis was performed on the COS eggshells to determine the C, N, O, and H elemental percentages with high precision using a Thermo Scientific Flash 2000.

Cytotoxicity assay

Cytotoxicity tests were performed with the L929 mouse skin fibroblast cell line (HUKUK, SAP Institute, Ankara, Turkey). The cells were cultured in Dulbecco's Modified Eagle Medium (DMEM) supplemented with 10% fetal bovine serum (FBS), penicillin (100 units/ml) and streptomycin (100 μg/ml). The cells were then seeded at 2×10^4 cells per well (96-well) and the culture plates incubated for 24 h at 37°C in a humidified incubator at 5% CO_2 before the cells were treated with the biomaterial. After 24 h, a 2 mm diameter section of the biomaterial was added to each well. The cultures were maintained under the same conditions for the incubation times (24, 48 and 72 h) without any medium change. The cytotoxicity of the biomaterial was evaluated by the classical MTT assay. Briefly, at the end of each incubation period, the culture supernatant was removed and the MTT solution (0.5 mg mL^{-1}) was added to each well and the plates incubated for 3 h at 37 °C in the dark. The MTT solution was then removed and DMSO was added to dissolve formazan crystals. After waiting 5 minutes for the color to stabilize, the absorbance at 492 nm was measured on a ChroMate® ELISA Reader.

Untreated cells, which contain no biomaterials, were considered as 100% and the measured viability values were normalized accordingly.

Data analysis

Data analysis was performed using GraphPad Prism software version 8 (GraphPad Software®). Data represent the mean – standard error of the mean (SEM). Statistical differences were evaluated by two-way ANOVA followed by a Bonferroni post-test.

SEM observation of L929 cells

To further examine the cytocompatibility of the eggshells, we conducted an SEM analysis of the morphology of L929 cells from the eggshells. Prior to analysis, cells grown onto these samples were washed with PBS, fixed with 4% paraformaldehyde for 30 min. The fixed samples were subsequently dehydrated with a series of increasing gradient ethanol solutions (20, 50, 70, 90 and 100% ethanol) and air-dried. Samples were gold-plated before analysis (Cressington 108 Auto sputter coated, Ted Pella, Inc.).

Atomic force microscope (AFM) measurements

Surface topography scans and mechanical properties of the outer and inner surfaces of the COS eggshells were obtained using a Multimode 8 AFM (Bruker Nano Surfaces, Santa Barbara, CA, USA) at ambient conditions. The surface scans were performed in tapping mode using PPP-NCHR cantilevers (Nanosensors, k=34 N/m, f=317 kHz) with a scan rate of 1 Hz. The recorded images were analyzed using Gwyddion 2.53 software (Czech Metrology Institute, Brno, Czech Republic) for calculating surface roughness from the root mean square (RMS) value. The mechanical properties (i.e., Young's modulus and adhesion force) of the COS eggshell inner and outer surfaces were measured with the force-volume (FV) mapping mode of the AFM with the probe used for surface topography scans. On 4 μm × 4 μm scanned areas of the FV maps,

16 × 16 force-distance curves were obtained by recording the interaction forces between the AFM probe and the substrate surface while the probe was approaching and retracting from the substrate. In total, 1200 and 2000 force-distance curves were recorded on the inner and the outer surfaces of three different eggshells, with a maximum applied load of 50 nN to ensure the indentation was less than 10% of the shell thickness. Each force-distance curve was processed by correcting the baseline offset and tilt of the curves as well as subtracting cantilever bending from the curves by using the NanoScope Analysis software of the AFM to convert the force-distance curves to force-indentation curves. From the force-indentation curves, the adhesion forces of the outer and inner surfaces of the COS eggshells were calculated as the lowest negative rupture force recorded when retracting the AFM probe from the substrate surface. The elastic property of the outer and the inner surfaces of the eggshells was obtained from the force-indentation curves by fitting the Johnson-Kendall-Roberts (JKR) model [31]. To stay within the JKR regime, we limited the indentation depths lower than the tip radius of the probe, which was measured as ca. 20 nm by imaging a reversed grid sample (TGT01, Micromash, Inc., Estonia).

In-situ growth of silver nanostructures

Two different strategies were used to initiate the growth of silver nanostructures on the eggshell surfaces. In both strategies, a growth solution was prepared containing 0.2 mM silver nitrate ($AgNO_3$; ≥99.5%; Sigma-Aldrich) and 0.4 mM hydroquinone (HQ; ≥99%; Sigma-Aldrich). In the first strategy, eggshells were immersed in the growth solution and shaken for 4 h in the dark, and then washed with distilled water and left to dry at room temperature. After an eggshell undergoes direct decoration with silver nanostructures, it is referred to as an “eggshell-Ag”. In the second strategy, aqueous solutions of rhodamine 6G (R6G, 99≥; Sigma-Aldrich) were first prepared at concentrations that ranged between 100 μM and 100 pM. The bare eggshells were

immersed in the R6G solution for 8 h, resulting in the absorption of R6G, due to the strong dye absorption characteristic of insect eggshells. A dye absorbed eggshell is referred to as an "eggshell-R6G". The growth of silver nanostructures was then performed on eggshell-R6G as described above. The resulting samples are referred to as "eggshell-R6G-Ag".

SERS analysis

R6G was used as the probe molecule in this study. Aqueous solutions of R6G were prepared at different concentrations that ranged from 100 μM to 100 pM. The R6G solution was dripped onto the eggshell-Ag and allowed to dry. SERS measurements were then taken on the dried eggshells. The SERS spectra were obtained using a confocal Raman spectrometer (WITec Alpha 300 M+, Germany) equipped with an excitation laser with 532 nm wavelength, where the laser beam is directed at the sample through a 50× objective (NA=0.85) with a working distance (WD) of 0.54 mm. The laser beam (5 mW) was focused on the substrate. Raman mappings were recorded with 1 μm steps using the integrated area of the baseline-corrected peaks at a position of 1653 cm^{-1}.

Antimicrobial assay

The antimicrobial effect of the insect eggshell was determined using *Escherichia coli* ATCC 25922 (Gram-negative) and *Staphylococcus aureus* ATCT 25923 (Gram-positive) bacteria. Initially, *E. coli* and *S. aureus* were cultured on Mueller-Hinton (MH) agar plates at 37 °C for 16-18 h. Afterwards, single colonies were selected and inoculated in 5-7 mL of Mueller-Hinton (MH) broth culture medium and shook at 250 rpm for 16-18 h at 37 °C. Bacterial inocula with an optical density of approximation of 1.5 x 10^8 cfu/mL, corresponding to the 0.5 McFarland standards, were prepared from the fresh cultures and then diluted to 1:100 in sterile MH broth. 20 mg silver-coated insect eggshells and non-silver coated insect eggshells were incubated at 37 °C for at least 72 h in 5 mL of MH broth. After incubation, the culture supernatant from each

tube was decanted, and the non-attached cells removed by washing the tubes with PBS (phosphate-buffered saline). Bacterial cells were fixed at 2.5% glutaraldehyde in PBS for 1 h and then washed with PBS. They were then fixed for 30 min in each concentration of a graded series of ethanol (50-100%) and then allowed to dry. Finally, bacterial attachment and biofilm formation on the eggshell surfaces were examined by a SEM (Leo 440 computer-controlled digitally).

Results and discussion

Natural assembly and characterization of the eggshell

A schematic representation of the COS egg structure is shown in Fig. 1. The outer surface of the eggshell consists of ordered hexagonal shapes, each with a series of 5 to 9 holes (= aeropyles) on the elevated frame of the hexagonal structure (Fig. 2A), in direct proportion to the size of the diameter of the hexagon. There are oval depressions with diameters of 20 - 80 μm in the middle of the hexagonal frames (Fig. 2A). The interior of the shell is lined with a smooth surface (Fig. 2B). When a cross section of the shell is examined, three different layers are found between the outer hexagonal structure and the smooth inner surface (Fig. 2C). There is a thick layer (23 μm ± 0.14) immediately below the hexagonal outer surface (referred to as Layer 1) (Fig. 1 green colour). Layer 1 consists of fan-shaped sheets approximately 5 μm in size. In addition, there are nanopores (about 200 nm) in the middle of each of the fan-shaped structures. Layer 2 (Fig. 1 red colour) is a laminar form consisting of stone-like flat pieces arranged in parallel layers with a thickness of 15 μm ± 0.37. Layer 3 is very narrow (700 nm ± 46) and consists of columnar structures (Fig. 1 blue colour).

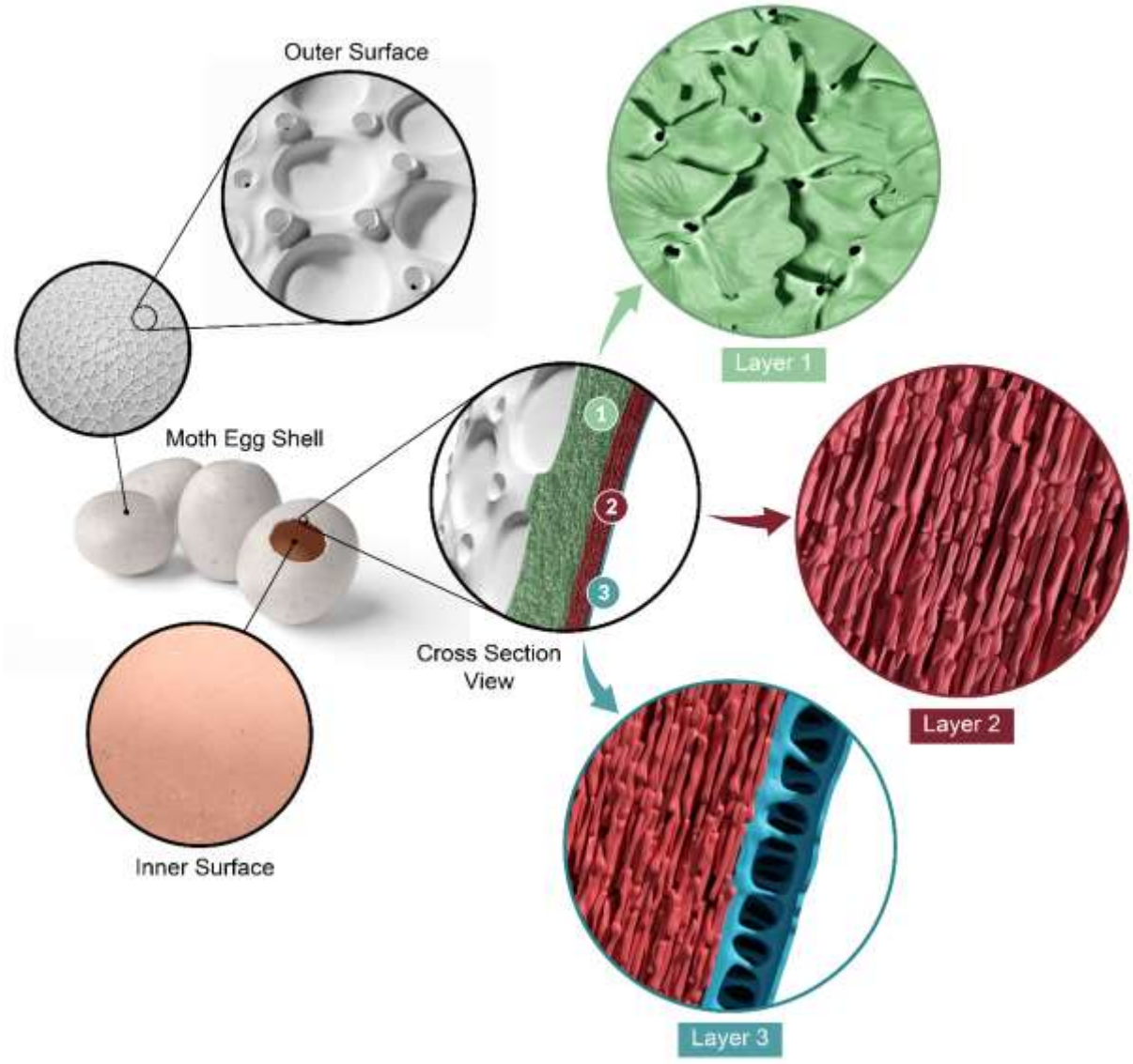

Figure 1. The schematic illustrations of the eggshell of Chinese oak silkworm (*Antheraea pernyi*) at macro, micro and nano scales. The white colour shows the outer surface of the eggshell. Rose gold colour represents the inner surface of the eggshell. Layers 1, 2 and 3 are illustrated with green, red and blue colours, respectively.

The unique morphology of eggshells was documented decades ago in a handful of studies [4,6,10,32]. It has been reported that insect eggshells are composed of multiple layers when viewed in cross section [4,5,7,33], although there has not been a consensus on the number of layers with different morphologies or a system for naming them. In the present study, detailed SEM images of the COS eggshell morphology revealed the distinct layers as shown in Fig. 1 and 2. These detailed analyses provide a valuable groundwork for future studies on the morphology of insect eggs.

The FTIR spectrum is given in Fig. 2D. Amide I, Amide II, and Amide III bands are characteristic of proteins and polypeptides [34]. These bands were recorded as 1624 cm^{-1}, 1510 cm^{-1}, and 1224 cm^{-1}, respectively, for the COS eggshell. Amide bands are also secondary structure indicators for proteins [35]. Peaks recorded as 1610-1640 cm^{-1} for Amide I represent β-sheet structure [34,36-38]. Similarly, the Amide III band recorded for the COS eggshell overlaps with the β-sheet structure peaks [39]. The detailed bands and their assignments are provided in Table S1. These results are consistent with the two different species of Lepidoptera (*Pericallia ricini* (Fabricius, 1775) (Lepidoptera: Arctiidae) and *Ariadne merione* (Cramer, 1777) (Lepidoptera: Nymphalidae)) chorion protein FTIR bands that have been previously analysed [40]. It has been reported that β-sheet structures are most probably antiparallel [40]. The presence of β -sheet structures provide strong mechanical properties to the structure [41,42]. These properties can be predicted to play an important role in the chorionic protein, whose main function is to protect the embryo from external agents during development.

Results of the TG/DTG analyses of COS eggshells are provided in Fig. 2E. As seen in the Figure, the mass loss occurred in two steps. The first loss (5.14%), which occurred between room temperature and 150°C, was due to the evaporation of the water in the structure. The second loss of 82.98%, occurring between 150 and 700°C, was due to degradation of the chorion protein, with maximum degradation recorded at 300°C. After heating the eggshell samples to 700°C, 10.61% ash remained. No information is available regarding the thermal properties of chorion protein. Maximum degradation temperatures of other structural proteins such as collagen, keratin and fibroin are known to be ca. 330°C [43-45]. Therefore, it can be concluded that the chorion protein has a lower thermal stability than other commonly known structural proteins.

The elemental profile (nitrogen, carbon, hydrogen, and sulphur) of the COS eggshell chorion protein was determined using two different analyses. In the first analysis using Thermo Flash 2000, the elemental composition of the chorion protein was determined as 14.22% nitrogen, 48.17% carbon, 6.24% hydrogen, and 2.11% sulphur. Elemental composition results based on EDS analysis are given in Fig. 2F. When the results of the two elemental analyses were compared, the nitrogen contents were similar, while the carbon content was higher in the EDS analysis. The amounts of *C* and *N* in proteins depend on their location as well as their chemical nature [46]. Previously reports [47] that chorion proteins can contain sulphur, phosphate, and calcium, were confirmed in the present study (Fig. 2F).

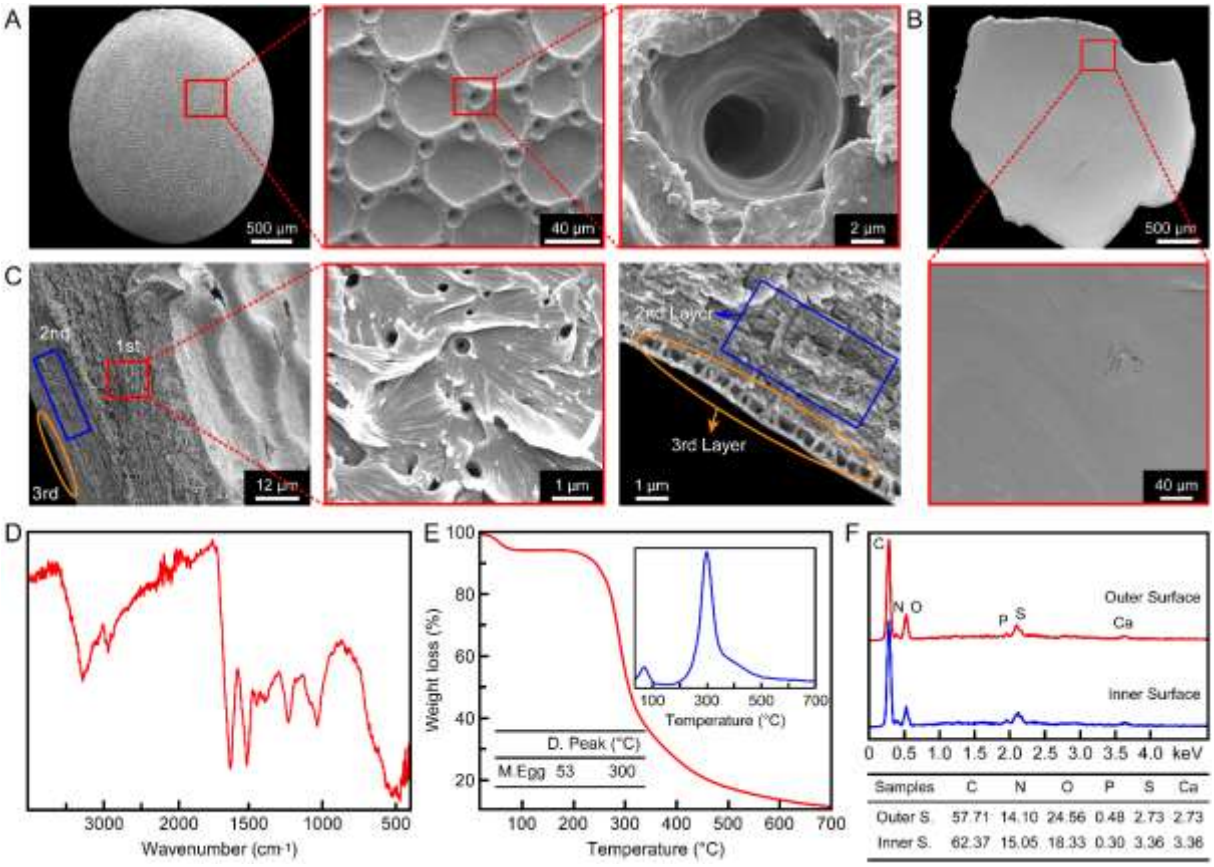

Figure 2. SEM images of the outer (A) and the inner (B) surface of the moth eggshell. (C) SEM images of the cross-sectional cut of the eggshell. (D) FT-IR spectrum of the eggshell. (E) TG/DTG of the eggshell, (F) EDS results of the eggshell taken from inner and outer surfaces. More SEM images of the eggshells are given in Fig. S2.

Surface morphologies and mechanical properties of the outer and the inner surfaces of COS eggshells characterized by AFM are demonstrated in Fig. 3. Using 50 μm × 50 μm scans (Fig. 3A), the frame height of the hexagonal structures at the outer surface was determined to be ca. 4 μm (inset of Fig. 3A). The surface roughness was calculated from 10 μm × 10 μm scans as 52 nm, and 25 nm for the outer and the inner surfaces of the eggshell, respectively (Fig. 3B-C). The Young's moduli of the outer and the inner surfaces obtained by AFM nanoindentation are shown in Fig. 3D-E as distributions. By fitting a Gaussian function to the overall histogram, Young's modulus of the outer surface was determined as 31.9 MPa (Fig. 3D), while an order of magnitude increase (to 548.2 MP) occurred in Young's modulus for the inner surface of the eggshell (Fig. 3E), emphasizing that the inner surface is much stiffer than the outer surface of the eggshell. The structural differences noted between Layer 1 and Layer 3 (shown in Fig. 1 and Fig. 2C) underneath the outer and the inner surfaces may explain the elastic modulus difference between these surfaces. From the statistical distributions of the measured adhesion forces shown in Fig. 3F, the mean adhesion force was 2.6 nN for the outer surface (red bars), and 10.5 nN for the inner surface (black bars) of the eggshell. The high-resolution AFM topography scans on the two eggshell surfaces (Fig. 3B-C) indicate that the outer surface is ~50% rougher than the inner surface. Therefore, the observed decrease in the adhesion force for the outer surface of the shell is likely attributed to an increase in the surface roughness.

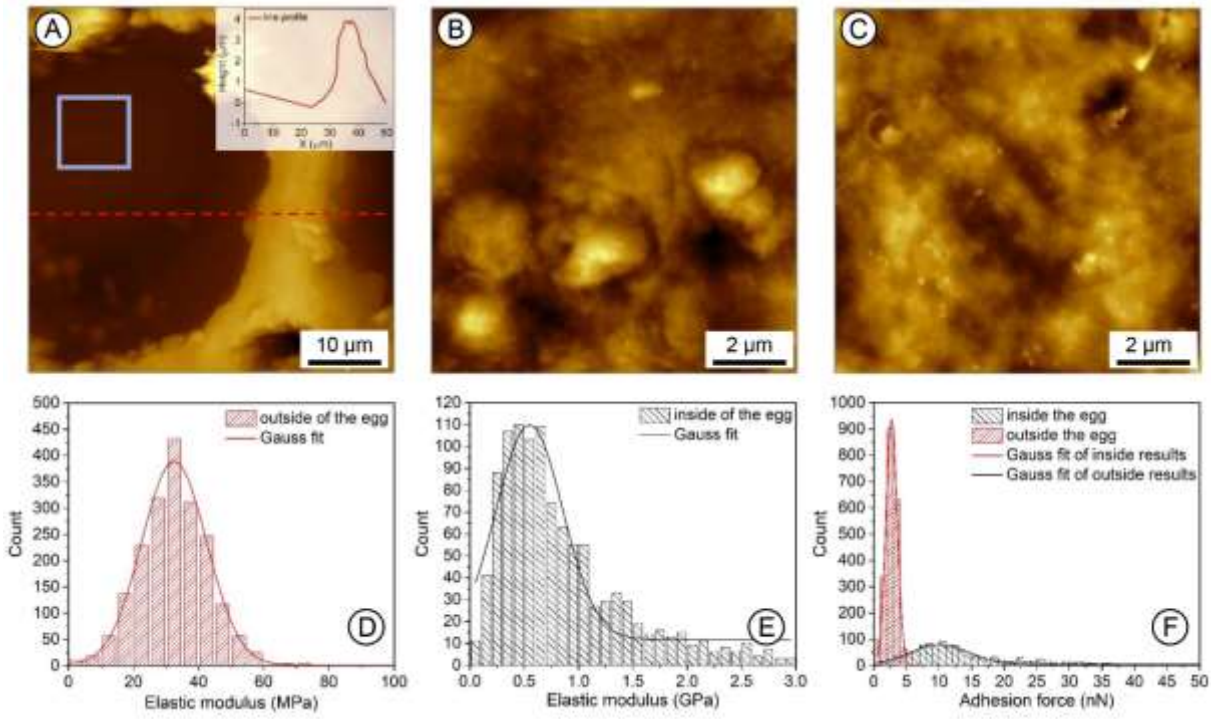

Figure 3. AFM topography images recorded on (A-B) outer and (C) inner surfaces of the COS eggshells (color scale ranges: 5.90 µm, 191 nm, and 89 nm, respectively). The inset of (A) represents the corresponding height profile along the dotted red line. The blue box highlights the location of area scanned in the subsequent topography image (B). The calculated root-mean-square (RMS) roughness value from high-resolution AFM topography images (B,C) are 52 nm, and 25 nm for outer and inner surfaces, respectively. Histograms present the distribution of (D,E) Young's modulus, and (F) adhesion forces recorded on outer (red bars) and inner (black bars) surfaces.

The interesting surface morphology and rich chemistry of insect eggshells offer a suitable template for the fabrication of SERS-active surfaces. To impart plasmonic activity, the surface of insect eggshells was decorated with silver nanostructures. For this purpose, hydroquinone (HQ), which has recently attracted growing interest in surface-growth of metallic nanostructures [48-50] was chosen as a reducing agent. HQ is a seed-selective reducing agent, which enables the controllable growth of metallic nanostructures on top of structured surfaces. We hypothesized that the outer surface of the insect eggshell could provide the necessary seed-like structures to enable the high-density growth of silver nanostructures. To facilitate the formation of plasmonic hot spots and therefore boost the SERS activity, we investigated two strategies for HQ mediated decoration of the insect eggshell surface with silver nanostructures: direct growth and dye-assisted growth. Fig. 4 illustrates schematic descriptions and key results. In the first strategy (direct growth) (Fig. 4A-D), the insect eggshell was simply placed in the

growth solution composed of the metal salt and HQ that resulted in the embellishment of the insect eggshell with silver nanostructures. These samples that were prepared using the first strategy were referred to as eggshell-Ag. In the second strategy (dye-assisted growth) (Fig. 4 E-H), we took advantage of the dye absorption characteristic of the insect eggshell. For this purpose, the insect eggshells were dipped into the solution of rhodamine 6G (R6G) resulting in samples that were referred to as eggshell-R6G. The process of silver growth was then performed on eggshell-R6G and the resulting samples were referred to as eggshell-R6G-Ag.

In the direct growth approach, silver nanostructures formed on the outer surface of eggshells as evidenced by the SEM images (Fig. 4B). The composition of the resulting metallic nanoparticles was further confirmed by EDX analysis (Fig. S3). To probe the SERS-activity of eggshell-Ag, an aqueous solution with an R6G concentration of 100 μM was dropped on the outer surface. The SERS spectrum (Fig. 4D) clearly shows the fingerprint vibrations of R6G: C-C-C ring in-plane bending at 615 cm^{-1}, C-H out-of-plane bending at 776 cm^{-1}, C-H in-plane bending at 1127 and 1185 cm^{-1}, aromatic C-C stretching at 1313, 1364, 1424, 1511, 1575 and 1673 cm^{-1}. The positions of these bands are a close match with those from the literature [51]. The mapping of the SERS-activity of the surface shows that the intensity of signals is higher near the edges of the hexagonal structures. This observation is in good agreement with the seed-mediated growth mechanism, which results in enhanced growth of silver nanostructures near edges [13,52].

To further increase the surface coverage of silver nanostructures and improve the SERS activity, we used the dye-assisted growth strategy. Polypeptide and protein structures are known to readily absorb dye molecules as a result of electrostatic and van der Waals interactions [53,54]. Based on this information, the second strategy began with absorption of R6G. The eggshell had completely absorbed the R6G molecules after 8 h. The red color (Fig. S4A) noted in eggshell-

R6G was the first visible indication of the strong absorption of the dye molecule. The surface of the eggshell-R6G were then decorated with silver nanostructures by immersion into the HQ and silver salt growth solution. A high-density growth of silver nanostructures on the surface of an eggshell-R6G-Ag can be seen in the SEM images (Fig. 4F). The red eggshell turned brown after the growth of silver (Fig. S4B). EDX analysis on the outer surface of eggshell-R6G-Ag further confirmed the presence of silver (Fig. S3B). The intensity of characteristic vibrations of R6G was significantly higher in eggshell-R6G-Ag compared to eggshell-Ag. This result suggests that the growth of silver nanostructures with high surface coverage favors the formation of plasmonic hot-spots. An explanation for the enhanced growth of silver nanostructures on the eggshell-R6G-Ag may involve the following potentialities: HQ is a weak reducing agent requiring a seed in order to reduce silver ions [55]. It is possible that dye molecules absorbed within the eggshell can act as seeds for highly efficient reduction of silver ions and effective growth of silver nanostructures. The electrostatic interaction between chloride ions in R6G and silver ions can further facilitate reduction of metal ions.

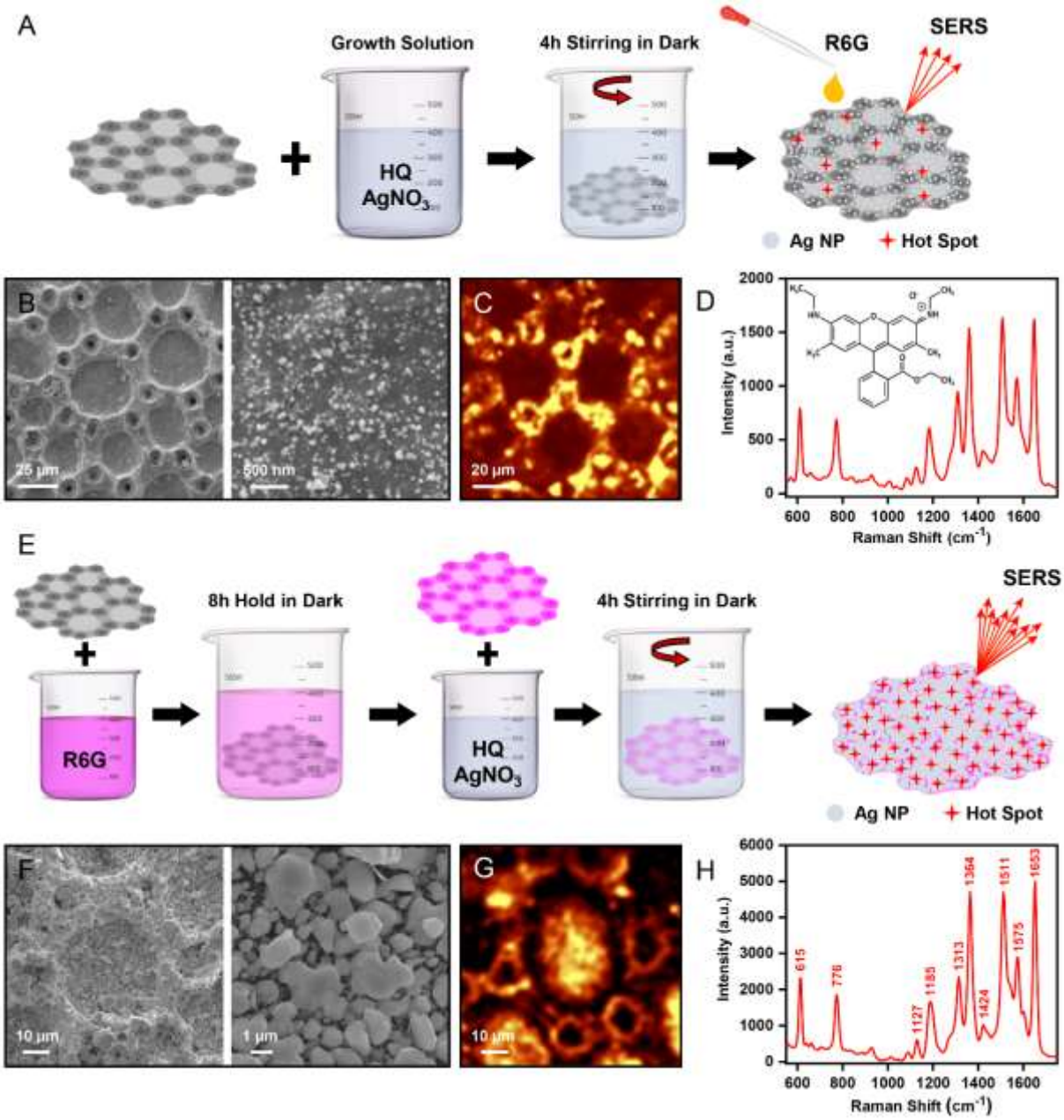

Figure 4. Surface growth of silver nanostructures and SERS activity. (A-D) Direct growth strategy. (A) Schematic illustration. (B) SEM images of an eggshell-Ag. (C) Raman mapping on an area 100 × 100 μm^2 for 100 μM R6G, (D) SERS spectra of 100 μM R6G (Inset: chemical structure of R6G) on eggshell-Ag. (E-H) Dye-assisted growth strategy. (E) Schematic illustration. (F) SEM images of eggshell-R6G-Ag. (G) Raman mapping on an area 50 × 50 μm^2 for 100 μM R6G, (H) SERS spectra of 100 μM R6G on an eggshell-R6G-Ag. Raman mapping images were generated using the band positioned at 1653 cm^{-1}.

To evaluate the SERS performance of eggshell-R6G-Ag, an analytical enhancement factor (AEF) was calculated using the following equation [49,56]:

$$AEF = \frac{I_{SERS}/C_{SERS}}{I_{Raman}/C_{Raman}} \quad (1)$$

Where I_{SERS} and I_{Raman} are the peak intensity at 1653 cm^{-1} of the Raman spectrum of R6G obtained on the SERS-active substrate and Si wafer, respectively. C_{SERS} and C_{Raman} are the concentration of R6G dropped on the SERS-active substrate and Si wafer, respectively. In the present study, I_{SERS} and I_{Raman} values were 91 and 147, respectively, while C_{SERS} and C_{Raman} values were 10^{-10} M and 10^{-3} M (Fig. S5). The AEF value was calculated as 6.2×10^{6}. This value is comparable or higher than SERS-active substrates obtained using different groups of insects [57-60]. An important modification used in this study is that the SERS-active substrate was obtained by a batch wet-chemical processing of the insect eggshell, whereas previous studies used costly vacuum processes such as physical vapor deposition to deposit metallic films.

Antimicrobial assay

We investigated whether bacteria could bind to the insect eggshell surface. Surprisingly, we found that each of the two bacteria tested (*E. coli* and *S. aureus*) attach to both eggshell surfaces (Fig. 5 A and B). We concluded that the insect's original eggshell has a microbial property and bacteria often form a film on both surfaces. Such bacterial films are of great importance in skin repair treatments for burns, wounds, ulcers, etc. [61]. After the silver coating was added to the outer surface during the SERS experiments, the outer surface became antimicrobial due to the silver coating (Fig. 5 C and D) [62]. Antimicrobial surfaces, on the other hand, are highly desirable features, particularly in the food industry [63]. The insect egg surface can possibly be used as a prototype for creating bacterial films and also has the potential to be used in the food industry as an alternative to silver coating.

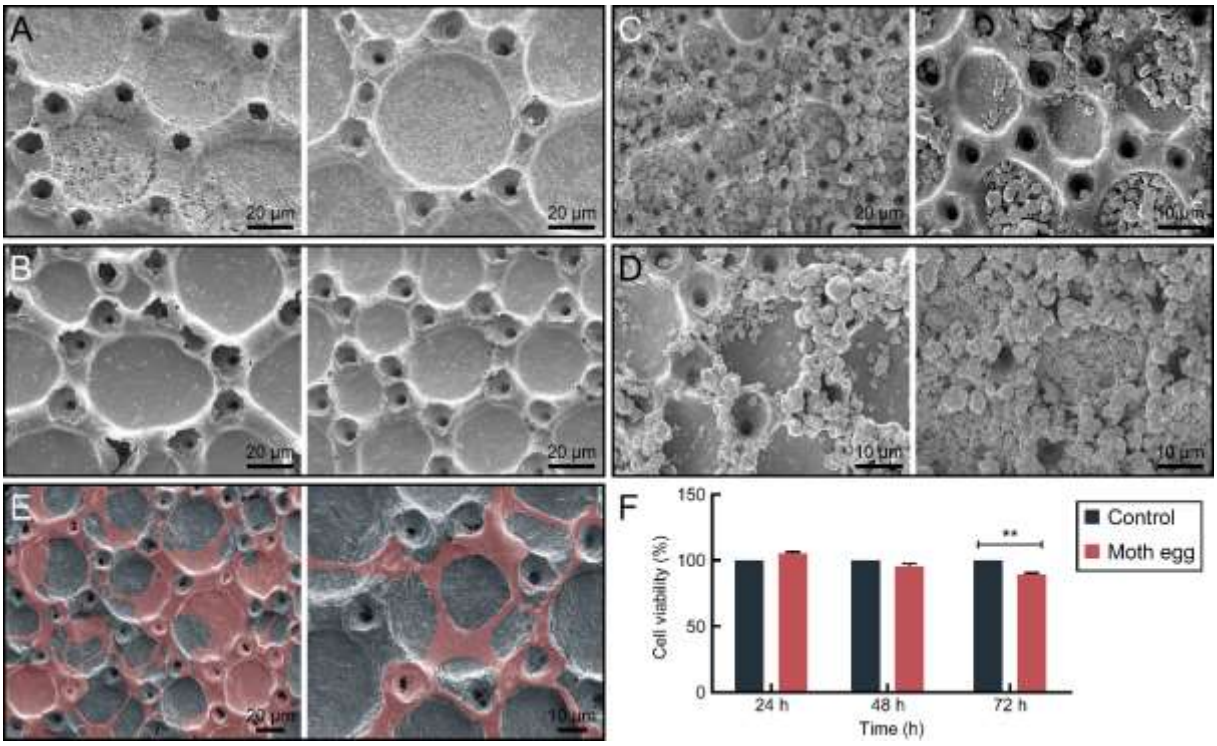

Figure 5. (A) SEM images of *E. coli* on the eggshells of Chinese oak silk moth. The film formation is visible on the surface of the eggshells. (B) SEM images of *S. aureus* on the eggshells of Chinese oak silk moth. More SEM images on the bacterial growth are given in Fig. S6. (C) and (D) Silver coated eggshell surfaces. As is seen from the images, there is no bacterial growth on the silver coated surfaces. (E) SEM images show the attachment of L929 cells on the outer surface of the eggshell (The false colored image shows the cells). (F) Cell viability assays of L929 cells after cultured with Moth egg for 24, 48, and 72 h. (Bar represents mean of cell viability ± SEM; n=3 statistical difference is regarded as ** $p < 0.05$).

Cell attachment and cytotoxicity assay

The biocompatibility of the material was evaluated by SEM analysis. SEM images of the L929 cells can be seen in Fig. 5E. Cells in the eggshell showed superficial attachment and bridging. On the basis of the behavior of the cells on this material, it was concluded that the eggshell is a biocompatible material capable of being used for varying applications. Cytotoxicity test results of L929 cells that were incubated with eggshells for 24, 48 and 72 h were estimated with MTT analysis. At 24 h, the viability of control cells (with only medium) and containing eggshells was determined as 100% and 105.7%, respectively. After 48 h incubation, the viability of cells was determined as 100% and 95.43% respectively. The viability of the cells changed to 100%, 86.48% after 72 h (Fig. 5F). No cytotoxicity was observed in the cells (all values > 70 %).

Conclusion

The eggs of *A. pernyi* moths, which are commonly used to culture the parasitoids used in many biological control programs, are generally considered to be large-scale bio-waste after emergence of the parasitoids. In the present study, the morphology of the eggshells was studied in detail at a nanoscale level, demonstrating the microstructural and physiochemical components of the shell's diverse structures. In summary: i) the shells are composed of chorion protein, ii) although the interior surface of the eggshell is smooth, the exterior consists of (semi)perfect hexagonal structures, iii) the eggshells are non-toxic, and, iv) the elastic modulus of the inner surface of the eggshell was shown to be substantially greater than the outer surface. Due to the unique surface morphology of the COS eggshells, it was determined that the discarded shells had an innate template potential for SERS applications. A cost-effective batch type process was developed to convert the eggshells to SERS active surfaces. The ability to render the surfaces as microbial or antimicrobial is an important consideration in addressing the needs of biocompatibility for a given application. In conclusion, it is hoped that these results may stimulate new studies in the field of materials science thanks to the excellent surface morphology and biological properties of the COS eggshells.

Acknowledgments

Thanks to ASUBTAM (Aksaray University) for providing laboratory facilities and access to equipment.

References

[1] N.E. Stork, Annual review of entomology 63 (2018) 31-45.

[2] M. Paul, et al., Journal of Supramolecular Structure 1 (1972) 60-65.

[3] A.S. Roy, and D. Ghosh, Munis Entomology & Zoology 11 (2016) 596-612.

[4] H. Hinton, Scientific American 223 (1970) 84-91.

[5] P. Irles, and M.-D. Piulachs, Insect biochemistry and molecular biology 41 (2011) 101-108.

[6] H. Hinton, Annual review of entomology 14 (1969) 343-368.

[7] J.C. Regier, et al., Developmental biology 76 (1980) 286-304.

[8] A. Papantonis, et al., Annual Review of Entomology 60 (2015) 177-194.

[9] A.C. Spradling, Cell 27 (1981) 193-201.

[10] H. Fehrenbach, et al., Int J Insect Morphol Embryol 16 (1987) 201-219.

[11] M. Sakir, et al., ACS applied materials & interfaces 9 (2017) 39795-39803.

[12] A. Klinkova, et al., Chemical Society Reviews 43 (2014) 3976-3991.

[13] S. Pekdemir, et al., ACS nano 14 (2020) 8276-8286.

[14] B. Yan, et al., Acs Nano 3 (2009) 1190-1202.

[15] S. Dodson, et al., The journal of physical chemistry letters 4 (2013) 496-501.

[16] M. Li, et al., Analyst 140 (2015) 386-406.

[17] M.F. Cardinal, et al., Chemical Society Reviews 46 (2017) 3886-3903.

[18] C. Muehlethaler, et al., Analytical Chemistry 88 (2016) 152-169.

[19] Z. Lin, and L. He, Current Opinion in Food Science 28 (2019) 82-87.

[20] S. Xu, et al., ACS Applied Nano Materials 1 (2018) 1257-1264.

[21] S. Karabel Ocal, et al., ACS Sustainable Chemistry & Engineering 7 (2019) 4315-4324.

[22] S. Pekdemir, et al., Journal of Colloid and Interface Science 584 (2020) 11-18.

[23] E. Lenzi, et al., ACS sensors 4 (2019) 1126-1137.

[24] W. Li, et al., Journal of Economic Entomology 110 (2017) 1404-1411.

[25] J.J. Zhang, et al., Pest management science 74 (2018) 959-965.

[26] Y.-M. Chen, et al., Journal of Pest Science (2020) 1-11.

[27] C. Pu, and C. Liu, Acta Entomol. Sin. 11 (1962) 409-414.

[28] A. Iqbal, et al., Journal of Pest Science 92 (2019) 1261-1269.

[29] A. Iqbal, et al., Journal of Pest Science 93 (2020) 1347-1357.

[30] L.-S. Zang, et al., Annual Review of Entomology 66 (2021) 463-484.

[31] K.L. Johnson, et al., Proc. Math. Phys. Eng. Sci. 324 (1971) 301-313.

[32] H. Fehrenbach, International Journal of Insect Morphology and Embryology 18 (1989) 261-274.

[33] M. Mazzini, International Journal of Insect Morphology and Embryology 7 (1978) 205-214.

[34] D.C.C. Martínez, et al., Procedia engineering 200 (2017) 377-383.

[35] F. Dousseau, and M. Pezolet, Biochemistry 29 (1990) 8771-8779.
[36] D.C. Benaki, et al., International journal of biological macromolecules 23 (1998) 49-59.
[37] D. Wilson, et al., Biophysical journal 78 (2000) 2690-2701.
[38] X. Hu, et al., Macromolecules 39 (2006) 6161-6170.
[39] S. Cai, and B.R. Singh, Biophysical Chemistry 80 (1999) 7-20.
[40] A. Srivastava, et al., International journal of biological macromolecules 49 (2011) 317-322.
[41] N.J.-A. Chan, et al., Nature communications 11 (2020) 1-14.
[42] S. Keten, et al., Nature materials 9 (2010) 359-367.
[43] M.D. Chomachayi, et al., Journal of Polymers and the Environment 28 (2020) 1252-1264.
[44] P. Kakkar, et al., Materials Science and Engineering: C 45 (2014) 343-347.
[45] B.T. Mekonnen, et al., ACS omega 2 (2017) 5260-5270.
[46] K. Jena, et al., International journal of biological macromolecules 120 (2018) 255-262.
[47] H.E. Hinton, Biology of insect eggs, Pergammon Press., Oxford, 1981.
[48] S.K. Cha, et al., ACS Nano 9 (2015) 5536-5543.
[49] M. Sakir, et al., Microchemical Journal 154 (2020) 104628.
[50] M. Sakir, and M.S. Onses, Results in Physics 12 (2019) 1133-1141.
[51] P. Hildebrandt, and M. Stockburger, The Journal of Physical Chemistry 88 (1984) 5935-5944.
[52] M. Sakir, et al., ACS Applied Materials & Interfaces 9 (2017) 39795-39803.
[53] A.S. de León, et al., Materials & Design 131 (2017) 121-126.
[54] P. Hanczyc, et al., ACS Photonics 2 (2015) 1755-1762.
[55] S.T. Gentry, et al., Langmuir 25 (2009) 2613-2621.
[56] S. Salem, et al., Colloids Surf. A Physicochem. Eng. Asp. 589 (2020) 124436.
[57] G. Shi, et al., Optics Communications 425 (2018) 49-57.
[58] N. Zhao, et al., RSC advances 9 (2019) 21771-21776.
[59] M.Y. Lv, et al., Sensors and Actuators B: Chemical 209 (2015) 820-827.
[60] G.C. Shi, et al., Scientific Reports 8 (2018) 6916.
[61] G.F. Picheth, et al., International journal of biological macromolecules 104 (2017) 97-106.
[62] J.M. Corrêa, et al., International journal of biomaterials 2015 (2015)
[63] P. Appendini, and J.H. Hotchkiss, Innov Food Sci Emerg Technol 3 (2002) 113-126.